Original Article

JCBFM

Journal of Cerebral Blood Flow & Metabolism
1–13

DOI: 10.1177/0271678X261465851
journals.sagepub.com/home/jcbfm


Trifluoperazine reduces infarct size, restores neurovascular coupling, and improves early outcomes in experimental acute ischemic stroke

Réka Tóth[1,2*], Anna Törteli[1,2*], Melinda Szabó[2*], Noémi Kovács[3,4], Ildikó Horváth[4], Attila E Farkas[5], Rita Frank[1,2], Krisztián Szigeti[4], Ferenc Bari[6], István A Krizbai[5,7], Domokos Máthé[3,4], Ákos Menyhárt[1,2] and Eszter Farkas[1,2**]**

Abstract

Cerebral edema and neurovascular dysfunction are reliable predictors of outcome after acute ischemic stroke (AIS), yet effective targeted therapies remain limited. We investigated the therapeutic potential of trifluoperazine (TFP), an FDA-approved antipsychotic and calmodulin inhibitor that modulates astrocytic aquaporin-4 expression. TFP administered after recanalization in a mouse model of AIS reduced infarct volume and improved early neurological recovery. Importantly, TFP restored neurovascular coupling and enhanced cerebral blood flow responses to spreading depolarizations, indicating improved cerebrovascular function. Mechanistic studies in acute brain slice preparations demonstrated that TFP attenuates cytotoxic tissue swelling, suppresses spreading depolarizations, reduces aquaporin-4 expression and preserves neuronal integrity under osmotic stress. These findings suggest that transient modulation of astrocytic cytotoxic edema and vascular reactivity represents a viable strategy to improve early stroke outcomes. Given its established clinical use, TFP emerges as a promising candidate for therapeutic repurposing in AIS.

Keywords

Acute ischemic stroke, aquaporin-4, neurovascular coupling, spreading depolarization, trifluoperazine

Received 23 January 2026; Revised 15 June 2026; Accepted 19 June 2026

[1]HCEMM-USZ Cerebral Blood Flow and Metabolism Research Group, HCEMM Nonprofit Ltd., Szeged, Hungary
[2]Department of Cell Biology and Molecular Medicine, University of Szeged, Szeged, Hungary
[3]HCEMM-SU In Vivo Imaging Advanced Core Facility, Budapest, Hungary
[4]Department of Biophysics and Radiation Biology—HUN-REN TKI, Semmelweis University, Budapest, Hungary
[5]Institute of Biophysics, HUN-REN Biological Research Centre, Szeged, Hungary
[6]Department of Medical Physics and Informatics, University of Szeged, Szeged, Hungary
[7]"Aurel Ardelean" Institute of Life Sciences, Vasile Goldiș Western University, Arad, Romania

*Shared first authorship.
**Shared last authorship.

Corresponding authors:
Eszter Farkas, HCEMM-USZ Cerebral Blood Flow and Metabolism Research Group, Department of Cell Biology and Molecular Medicine, University of Szeged, Somogyi u. 4, Szeged H-6720, Hungary.
Email: farkas.eszter@szte.hu

Ákos Menyhárt, HCEMM-USZ Cerebral Blood Flow and Metabolism Research Group, Department of Cell Biology and Molecular Medicine, University of Szeged, Somogyi u. 4, Szeged H-6720, Hungary.
Email: menyhart.akos@szte.hu

Introduction

Acute ischemic stroke (AIS) remains a serious health concern, as its incidence, mortality, and associated disability have lately risen substantially worldwide.[1] On top of the primary impact caused by the obstruction of a cerebral blood vessel, ATP depletion during AIS triggers a cascade of secondary pathophysiological processes that occur concurrently with or following the primary occlusion. Among the various comorbid complications of AIS, cerebral edema is a key prognostic indicator of injury progression and unfavorable outcome in stroke patients.[2] Indeed, the evolution of cerebral edema correlates strongly with infarct expansion,[3] and the stroke-related mortality rate rises to approximately 80% when malignant brain edema develops.[4]

Currently available hyperosmotic treatments (e.g. bolus hypertonic saline or mannitol)[5] can exert adverse effects, such as acute hypotension, electrolyte imbalances,[6] endothelial dysfunction, and disruption of the blood–brain barrier (BBB).[7] Moreover, conventional interventions are typically reactive rather than preventive. Importantly, these therapies mainly target vasogenic edema (the movement of water from the vascular network into the brain parenchyma) rather than cytotoxic edema (the influx of water into cells from the interstitium), despite evidence that cytotoxic edema is an early event following brain injury, precedes vasogenic edema, and promotes its subsequent formation.[8,9]

Alternative, more targeted anti-edema therapies may focus on aquaporin-4 (AQP4) water channels, which are abundantly expressed in astrocytes throughout the brain.[10] AQP4 expression is especially prominent at astrocytic perivascular endfeet, where the channels mediate osmotically driven, bidirectional water movement between the bloodstream or cerebrospinal fluid in perivascular spaces and the brain parenchyma.[11–13] AQP4 plays a central role in the development of cytotoxic edema, as demonstrated by studies in AQP4 knockout mice, in which ischemia-induced brain swelling was reduced by approximately 35% compared with wild-type controls.[14] For these reasons, pharmacological modulation of AQP4 has emerged as a promising strategy to limit brain edema formation by restricting pathological water influx. AQP4 is an especially attractive target for cytotoxic edema reduction because its water transport function is closely linked to the spatial buffering of K^+ that accumulates in ischemic brain tissue[11] and may be upregulated by inflammatory mediators, such as interleukins released after ischemia.[15] Furthermore, the efficacy of transmembrane water flux is enhanced when AQP4 physically co-assembles with cation channels in lipid rafts at the astrocyte membrane.[16] Notably, the sulfonylurea receptor 1 (SUR1)-transient receptor potential melastatin 4 (TRPM4)–AQP4 complex has been identified as a major route of bulk water influx driving astrocyte swelling.[17]

Direct pharmacological blockade of AQP4, however, may be counterproductive, because AQP4 contributes not only to cytotoxic edema formation but also to edema resolution.[18] As an alternative approach, reversible modulation of AQP4 subcellular localization focused on the hyperacute phase of injury, rather than pore blockade, has been proposed. This concept is supported by observations showing that both AQP4 expression and its membrane distribution are altered in astrocytes exposed to hypotonic stress and in the mouse cortex following acute brain injury.[19,20] In primary cortical astrocyte cultures, exposure to hypotonic conditions or mechanical impact increased the relocation of AQP4 from intracellular vesicles to the plasma membrane.[20,21] These findings suggest that AQP4 becomes more abundant on the astrocyte surface during acute injury and contributes to edema formation. Therefore, inhibiting AQP4 translocation to astrocytic endfeet during the hyperacute phase of AIS may prove beneficial.

The translocation of AQP4 from intracellular vesicles to the plasma membrane has been linked to increases in intracellular Ca^{2+} concentration and the activation of Ca^{2+}-dependent calmodulin.[18] Notably, AQP4 translocation to the astrocytic membrane was inhibited by trifluoperazine (TFP), a calmodulin antagonist and, importantly, an FDA-approved antipsychotic agent.[22] Furthermore, TFP administration reduced edema formation and improved functional outcomes in a rodent model of spinal cord injury.[22] Collectively, these findings suggest that pharmacological inhibition of AQP4 translocation to the astrocyte surface may represent a novel therapeutic approach for mitigating cerebral edema.[16]

Building on these lines of evidence, we hypothesized that TFP administration during the early phase of AIS could inhibit cytotoxic edema formation, limit infarct maturation, and improve functional recovery. To test this hypothesis, we administered TFP in a filament middle cerebral artery occlusion (MCAO) model in mice and assessed infarct size, edema formation and blood–brain barrier leakage using MRI and SPECT, evaluated neurological outcomes, and examined neurovascular coupling with somatosensory stimulation. Additionally, we investigated the brain's susceptibility to spreading depolarizations (SDs), electrophysiological events that occur in ischemic tissue and are thought to exacerbate infarct maturation in acute brain injury, including AIS.[23] The evolution of SD is confirmed to mediate the progression of cytotoxic edema formation after acute brain injury.[24] Importantly, SDs and the coupled cerebral blood flow (CBF) response also provided an opportunity to study neurovascular coupling. Finally, we extended our in vivo findings to acute, osmotically challenged brain slice preparations to validate TFP's anti-edema efficacy and to further characterize its mechanistic effects in a controlled ex vivo experimental system.

Materials and methods

Animals

Adult male C57BL/6 mice (Charles River Laboratories; 4–4.5 months old; weighing 26.83 ± 3.91 g) from the husbandry facility of the Biological Research Centre, Szeged, Hungary, were used in this study. All experimental procedures were approved by the National Food Chain Safety and Animal Health Directorate of Csongrád County, Hungary (ref. no. II./1234/2025) and conducted in strict accordance with its guidelines and those of the Scientific Committee of Animal Experimentation of the Hungarian Academy of Sciences (updated Law and Regulations on Animal Protection: 40/2013 (II. 14.) Gov. of Hungary), following EU Directive 2010/63/EU on the protection of experimental animals. The study adhered to established ethical guidelines, and the experiments are reported in compliance with the ARRIVE guidelines.[25] The animals were housed under controlled environmental conditions (temperature: 23 °C; humidity: constant; light/dark cycle: 12 h/12 h, lights on at 7 a.m.). Standard rodent chow and tap water were provided ad libitum. The animals were randomly allocated to the experimental groups and the datasets were coded so that the experimental conditions were not revealed.

Sample size estimation

Power analysis for the performed experiments followed established principles. The pilot experiments indicated differences between the experimental groups (TFP1/TFP5 vs control) and achieved the confidence level of 95% and a power of 80% at low sample size ($\alpha = 0.05$ and β (type II error) of 0.2). As calculated, sufficient statistical power was assumed at a final sample size of 8–10 animals/group. The calculations were run in GPower 3.1 (Heinrich Heine University of Düsseldorf, Germany).

Modified filament middle cerebral artery occlusion (MCAO)

Middle cerebral artery occlusion (MCAO) procedures were performed as previously described.[26] Briefly, mice ($n = 62$) were anesthetized with isoflurane (in O_2:N_2O, 1:2; 0.5%–1.5%), and body temperature was maintained at 37 °C. To confirm induction of ischemia, CBF was monitored using a laser Doppler probe (Probe 403, connected to a PeriFlux 5000; Perimed AB, Sweden) attached to the parietal bone over the cortical area supplied by the middle cerebral artery (MCA). Occlusion of the left MCA was performed according to a modified version of the Koizumi method.[26,27] After retracting the external carotid artery with surgical silk, a microclip (Fine Science Tools, Inc., USA) was placed on the common carotid artery. A silicone-coated 230-µm microfilament (Doccol Corporation, USA) was then advanced through a small incision in the internal carotid artery until it reached the origin of the MCA, indicated by a sudden increase in resistance. Successful occlusion was confirmed by a reduction in CBF to less than 20% of baseline. Reperfusion was induced 60 min later by gently retracting the filament and closing the carotid incision with a gelatin sponge under light compression. The microclip was removed from the common carotid artery, and the external carotid artery was released. Post-operative care adhered to previously established protocols.[26] In total, 41 mice survived for 72 h (66% survival rate) and were included in the data analysis. The mice were allocated to neurological testing and neuroimaging ($n = 23$) or to the evaluation of neurovascular coupling ($n = 19$).

Pharmacological treatment

For neurological testing and subsequent neuroimaging, three experimental groups were established based on treatment. The first group (TFP1; $n = 8$) received 1 mg/kg trifluoperazine (TFP) subcutaneously after complete recanalization of the middle cerebral artery (MCA), repeated every 24 h, with the final dose administered at 72 h post-surgery. The second group (TFP5; $n = 7$) received a single subcutaneous dose of 5 mg/kg TFP immediately after recanalization. The control group ($n = 8$) received vehicle (0.1% DMSO in saline) only.

Neurological testing

Animals underwent neurological testing 24 h before surgery and daily from 24 to 72 h after MCAO. The Garcia Neuroscore Scale (GNS), a scoring system designed to evaluate sensorimotor deficits following ischemic brain injury in rodents, was used.[26,28,29] The GNS score ranges from 0 (severe deficit) to 21 (no deficit). All test domains were performed in the same order for each animal, with three investigators present simultaneously to ensure unbiased scoring.

MRI and SPECT imaging

MRI and SPECT imaging were performed 72 h after MCAO. [^{99}mTc]-DTPA (76.03 ± 34.23 MBq) was administered intravenously via tail vein prior to imaging. During the 1-h incubation with the radiopharmaceutical, MRI scanning was performed as reported earlier,[26] using a Mediso NanoScan PET/MRI 3T system (Mediso Ltd., Budapest, Hungary) equipped with 450 mT/m maximum gradient strength. A dedicated mouse head volume coil (inner diameter: 30 mm) was used for both transmission and reception.

Animals were placed on a heated platform during scanning and anesthetized with 1%–2% isoflurane. Respiration rate and body temperature were continuously monitored,

and isoflurane concentration was adjusted as needed. T_2-weighted fast spin echo (T2FSE) scans were acquired using a three-dimensional acquisition scheme with the following parameters: field of view (FOV) = 35 × 35 mm, acquisition matrix = 220 × 220, and 96 contiguous slices of 0.2-mm thickness. The echo-train length was 96, echo time (TE) = 69 ms, repetition time (TR) = 2 s, with one average, yielding a total acquisition time of approximately 6.5 min.

Diffusion-weighted imaging (DWI) was performed with two *b*-values ($b = 0$ and 800 s/mm²; $\delta = 2.4$ ms; $\Delta = 12$ ms) along three perpendicular directions, each repeated 14 times. A spin-echo echo-planar imaging (SE-EPI) pulse sequence was used to acquire high-quality images of 22 adjacent slices (0.7-mm thickness) within a total acquisition time of 10 min. The FOV was set to 25 × 25 mm, with an acquisition matrix of 80 × 80. Echo time was 59.1 ms, bandwidth 300 kHz, and repetition time 5 s.

Susceptibility and eddy current distortion corrections were applied during image reconstruction based on reference echo scans. Apparent diffusion coefficient (ADC) values were calculated for the lesion area, the entire ipsilateral (stroke-affected) hemisphere, and the contralateral intact hemisphere using InterView Fusion software (Mediso, Hungary). Hemispheric volumes (HV) and lesion volumes (LV) were derived from T2FSE sequences and ADC maps.

MRI scans were immediately followed by SPECT/CT measurements performed on a nanoSPECT/CT system (Mediso Ltd., Budapest, Hungary) equipped with multi-pinhole collimators. Head SPECT scanning was conducted with 30 frames per cycle and a termination condition of 120 s per frame over a scan range of 26.8 mm. SPECT reconstruction was performed using 0.2-mm isotropic voxels, and the FOV was centered on the head. SPECT results were quantified as radioactivity concentration (MBq/ml). Image analysis was performed using VivoQuant software (inviCRO, Boston, MA, USA). Tissue volume with BBB leakage was determined by threshold-based segmentation of high-uptake regions on the [^{99}mTc]-DTPA SPECT images, and the activity concentration ratio between the injured and intact hemispheres was calculated.

Evaluation of neurovascular coupling

Neurovascular coupling (NVC) was assessed by measuring the magnitude of functional hyperemia in response to mechanical whisker pad stimulation. Seventy-two hours after MCAO, animals ($n = 19$) were anesthetized with isoflurane as described above. After securing the head in a stereotaxic frame and exposing the skull, a laser Doppler probe (Probe 403, connected to a PeriFlux 5000; Perimed AB, Sweden) was positioned over the barrel cortex ipsilateral to the prior MCAO. A silver ball electrode (Ag/AgCl; WPI Instruments, Sarasota, FL, USA) was placed nearby, and an Ag/AgCl reference electrode was implanted under the skin of the animal's neck. The instrumentation for electrophysiological recordings was identical to that described previously.[30] This configuration allowed for minimally invasive recording of EEG and CBF. Anesthesia was switched from isoflurane to medetomidine (0.1 mg/kg, i.p.), supplemented with a reduced concentration of isoflurane (0.1%) to maintain proper baseline vascular tone and sufficient analgesia. After achieving a stable baseline CBF, contralateral mechanical whisker stimulation was performed at a frequency of 2 Hz for 30 s and repeated three times with 2-min intervals to allow full recovery of CBF between stimulations. The procedure was then repeated in the contralateral, non-ischemic hemisphere, which served as the control. TFP-treated groups (TFP1, $n = 7$; TFP5, $n = 6$) were evaluated against controls ($n = 6$).

Susceptibility to spreading depolarization

A separate group of mice ($n = 16$) were anesthetized with isoflurane as described above and mounted in a stereotaxic frame. An open craniotomy over the parietal cortex was prepared for local field potential (LFP) recording and laser Doppler flowmetry, while a smaller, caudal trepanation was used to elicit SDs. The cranial windows were continuously superfused with artificial cerebrospinal fluid (aCSF; composition in mM: 126.6 NaCl, 3 KCl, 1.5 $CaCl_2$, 1.2 $MgCl_2$, 24.5 $NaHCO_3$, 6.7 urea, and 3.7 glucose), bubbled with 95% O_2 and 5% CO_2 to maintain a constant pH of 7.4.

Two glass capillary microelectrodes filled with saline (20 µm outer tip diameter, 1–3 MΩ) were inserted into the parietal cortex, with the reference electrode placed subcutaneously under the neck. The electrophysiological signal filtered in DC mode was recorded as described previously.[31,32] The amplified, conditioned and filtered signal was digitized using an analog-to-digital (A/D) converter (MP150, Biopac Systems, Inc., USA) and continuously recorded at a sampling rate of 1 kHz with AcqKnowledge software (version 4.2.0; Biopac Systems, Inc., USA).

Local CBF was recorded using a laser Doppler needle probe (Probe 403, connected to a PeriFlux 5000; Perimed AB, Sweden) positioned adjacent to one of the glass microelectrodes. The signal was digitized and acquired together with the DC potential, as described above.

After a 10-min baseline recording, both the acquisition and elicitation windows were incubated with 20 µM TFP solution prepared in aCSF for 20 min ($n = 8$). The solvent (aCSF) served as the control ($n = 8$). The solutions were renewed every 10 min. Spreading depolarizations were elicited after the incubation period by topical application of 1 M KCl to the caudal window, renewed every 15 min throughout the 120-min recording period.

Live brain slice preparations

Coronal brain slices were prepared as previously described.[33] Briefly, 350-µm-thick coronal slices ($n = 55$) from adult C57BL/6 mice were cut anterior to bregma using a vibrating-blade microtome (VT1000S, Leica Microsystems, Germany). Slices were collected in ice-cold modified artificial cerebrospinal fluid (aCSF; composition in mM: 130 NaCl, 3.5 KCl, 1 NaH_2PO_4, 24 $NaHCO_3$, 1 $CaCl_2$, 3 $MgSO_4$, and 10 D-glucose) and allowed to recover in carbogenated (95% O_2, 5% CO_2) normal aCSF (composition in mM: 130 NaCl, 3.5 KCl, 1 NaH_2PO_4, 24 $NaHCO_3$, 3 $CaCl_2$, 1.5 $MgSO_4$, and 10 D-glucose). Randomly selected slices were continuously perfused with carbogenated aCSF at a rate of 2.5 ml/min in an interface-type recording chamber (BSC1, Scientific Systems Design, Inc., ON, Canada) maintained at 32 °C using a temperature controller unit (PTC03, Scientific Systems Design, Inc., ON, Canada).

For intrinsic optical signal (IOS) imaging,[33,34] slices were illuminated with a halogen lamp (Intralux 5100, Volpi AG, Schlieren, Switzerland). Image sequences were recorded at 1 Hz using a monochrome CCD camera (Pantera 1M30; DALSA, Gröbenzell, Germany; spatial resolution: 1024 × 1024 pixels) mounted on a stereomicroscope (MZ12.5; Leica Microsystems, Wetzlar, Germany), providing 6×–10× magnification.

After establishing a baseline in aCSF, brain slices were incubated in hypo-osmotic medium (HM), prepared by reducing the NaCl concentration in the aCSF from 130 to 60 mM (corresponding to 339 and 199 mosm/l, respectively), which induces spontaneous SD.[33] A second SD was evoked 45 min after the onset of HM incubation by transient withdrawal of oxygen from the medium for 2.5 min.[32] Slices were then randomly assigned to either the TFP group (10 µM in 0.01% DMSO in aCSF) or the vehicle group (0.01% DMSO in aCSF). Following the experimental protocol, brain slices were immediately processed for 2,3,5-triphenyltetrazolium chloride (TTC) staining.[33,34]

Immunocytochemistry

To evaluate astrocyte reactivity, neuronal integrity, and aquaporin-4 expression, immunostaining for glial fibrillary acidic protein (GFAP), neuronal nuclei (NeuN), and aquaporin-4 (AQP4) was performed. After concluding the recording protocol, brain slices were transferred from the recording chamber to a glass vial and immersed and stored in 4% paraformaldehyde (PFA) for 24 h. Brain slice preparations (350 µm) were then paraffin-embedded and sectioned at 3 µm using a rotary microtome (Leica RM2235, Germany). Sections were mounted onto microscope slides. Following deparaffinization and rehydration, sections were blocked with 10% normal goat serum (Sigma–Aldrich, USA) at room temperature for 1 h and then incubated overnight at 4 °C with the following primary antibodies: mouse anti-GFAP (Sigma–Aldrich, G3893, 1:1500), rabbit anti-NeuN (Abcam, ab177487, 1:500), or mouse anti-AQP4 (Santa Cruz, sc-390488, 1:100). After rinsing in PBS, sections were incubated for 2 h at room temperature with the appropriate secondary antibodies: goat anti-mouse IgG (H + L) Alexa Fluor™ 568 (Thermo Fisher Scientific, USA, A-11031, 1:1000) for GFAP; goat anti-rabbit IgG (H + L) Alexa Fluor™ 488 (Thermo Fisher Scientific, USA, A-11008, 1:1000) for NeuN; or goat anti-mouse IgG (H + L) Alexa Fluor™ 568 for AQP4. Sections were then rinsed with PBS and distilled water, coverslipped with Fluoromount-G containing DAPI (Thermo Fisher Scientific, 00-4959-52), and stored at 4 °C. Fluorescent images were acquired using a Leica DFC250 camera (Leica Microsystems, Wetzlar, Germany) attached to a fluorescence microscope (Leica DM LB2) at 5×, 10×, 20×, and 40× magnification. Quantification of immunopositive area fractions for GFAP, NeuN, and AQP4 was performed in the cortex from randomly selected photomicrographs using threshold-based analysis in ImageJ Fiji. The immunopositive area fraction (%) was calculated as the ratio of the thresholded signal area to the total region of interest.

Data analysis and statistics

Data analysis followed previously established protocols.[26,30,31,33,34] Data are presented as mean ± stdev, with individual data points overlaid. The normality of data distribution was assessed using the Shapiro–Wilk test. Data sets with discrete values were analyzed using the Mann–Whitney test. For data sets showing a normal distribution, one-way ANOVA, two-way ANOVA, or repeated-measures ANOVA was applied, depending on the variables. ANOVA analyses were followed by Sidak-Holm's post hoc test. Statistical significance was set at $*p < 0.05$ and $**p < 0.01$. The specific statistical tests applied are indicated in each figure legend.

Results

TFP reduces infarct volume and attenuates neurological deficits

MRI performed 3 days after MCAO revealed distinct focal cortical and striatal infarcts in all experimental groups (Figure 1(a)), as indicated by hyperintense T2 signal with concurrent restricted diffusion in the affected areas. TFP administered in two treatment regimens reduced lesion volumes, particularly when given as a single, higher bolus dose immediately after recanalization (TFP5; 20.5 ± 15.6 and 32.0 ± 14.5 vs 52.5 ± 15.6 mm^3, TFP5 and TFP1 vs control; Figure 1(b)). Space-occupying edema accompanying ischemia, expressed as the increase in hemispheric

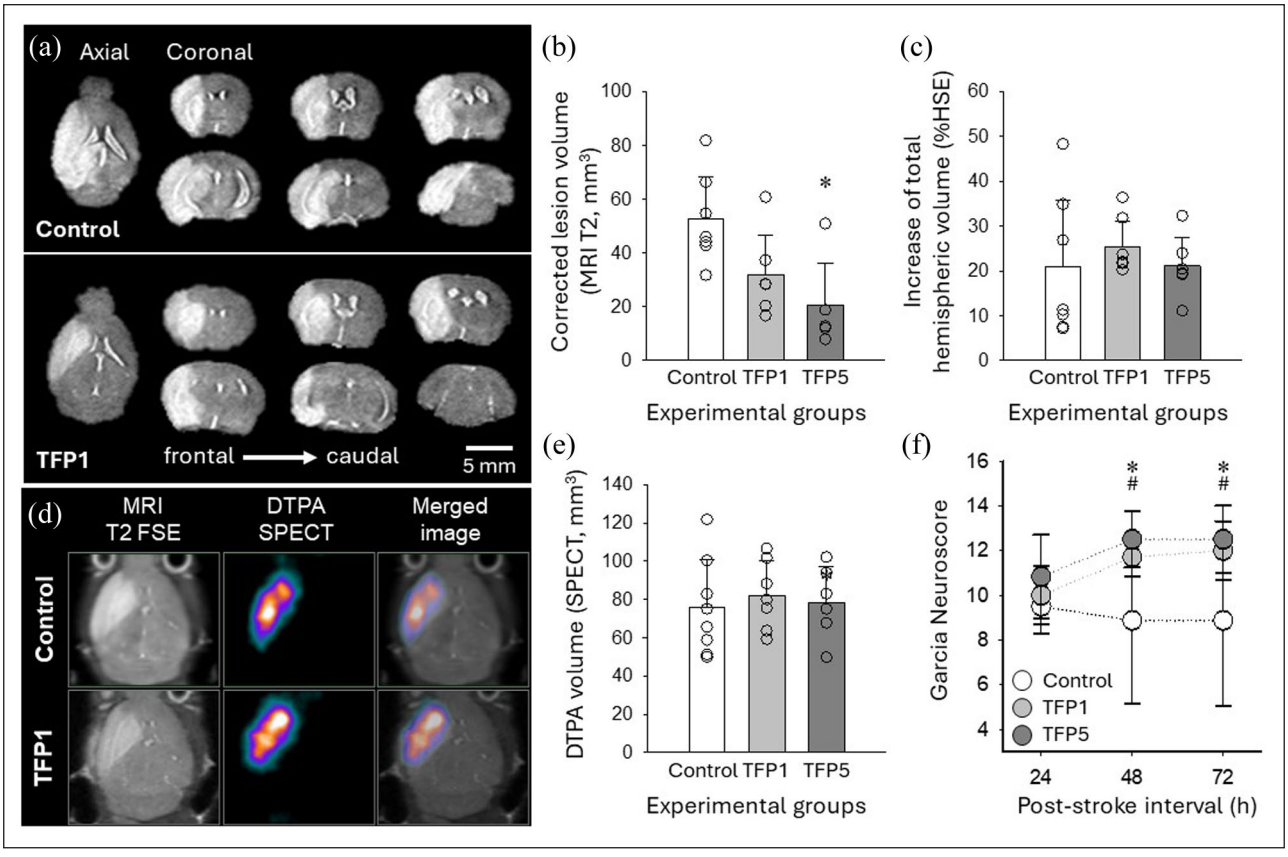

Figure 1. TFP reduces infarct volume and improves functional outcome but does not mitigate edema formation or blood–brain barrier leakage: (a) representative T2-weighted MRI images demonstrate infarct volume in the brains of a control and a TFP-treated mouse, (b) the protective effect of TFP is shown by the reduction in corrected lesion volume, (c) the increase in total hemispheric volume was not inhibited by TFP, (d) representative MRI T2-FSE and SPECT maps indicate DTPA uptake co-localized with the ischemic infarct, (e) the volume of DTPA-labeled tissue was similar across groups, and (f) TFP administration improved neurological function 48 and 72 h after focal cerebral ischemia. Data are presented as mean ± stdev, with individual data points overlaid. After confirming normal distribution using the Shapiro–Wilk test, a one-way ANOVA (b, c, e) or a repeated-measures ANOVA (f) followed by a Sidak–Holms post hoc test was applied for statistical analysis. Significance was set at $^{*}p < 0.05$ (TFP5 vs control) and $^{\#}p < 0.05$ (TFP1 vs control).
TFP: trifluoperazine.

volume (%HSE), did not differ between the TFP-treated groups and the control group (21.1% ± 6.3% and 25.4% ± 5.7% vs 20.9% ± 14.9%, TFP5 and TFP1 vs control; Figure 1(c)). Finally, SPECT scans were performed immediately after MRI acquisition to assess blood–brain barrier (BBB) permeability (Figure 1(d)), as elevated DTPA uptake indicates BBB leakage and associated vasogenic edema. Although tracer accumulation suggesting BBB disruption was evident within the infarcted areas (Figure 1(d)), no treatment effect was observed (78.6 ± 18.8 and 82.1 ± 17.9 vs 75.7 ± 25.2 mm^3, TFP5 and TFP1 vs control; Figure 1(e)).

Infarct volumes evaluated by neuroimaging corresponded with neurological test results in our cohort of animals. Although all mice were equally impaired 24 h after MCAO, as reflected by GNS values averaging 9–10 (with 21 indicating normal performance), both TFP-treated groups showed improvement from the second post-operative day, with group averages increasing to 12–13 points compared with 10–11 points in the control group (Figure 1(f)).

TFP restores functional hyperemia after AIS

We tested whether TFP restores cerebrovascular reactivity after AIS by measuring the amplitude of functional hyperemia in response to mechanical whisker stimulation. As expected, functional hyperemia evoked by somatosensory stimulation was virtually abolished after AIS, as shown by the relative amplitude of the response (4.0% ± 3.2% vs 20.9% ± 7.1%; control stroke vs control intact hemisphere; Figure 2(a) and (b)). Importantly, administration of TFP at both doses restored the amplitude of functional hyperemia to near-control values (19.4% ± 5.5% and 20.0% ± 12.9% vs 20.9% ± 7.1%; TFP1 stroke and TFP5 stroke vs control

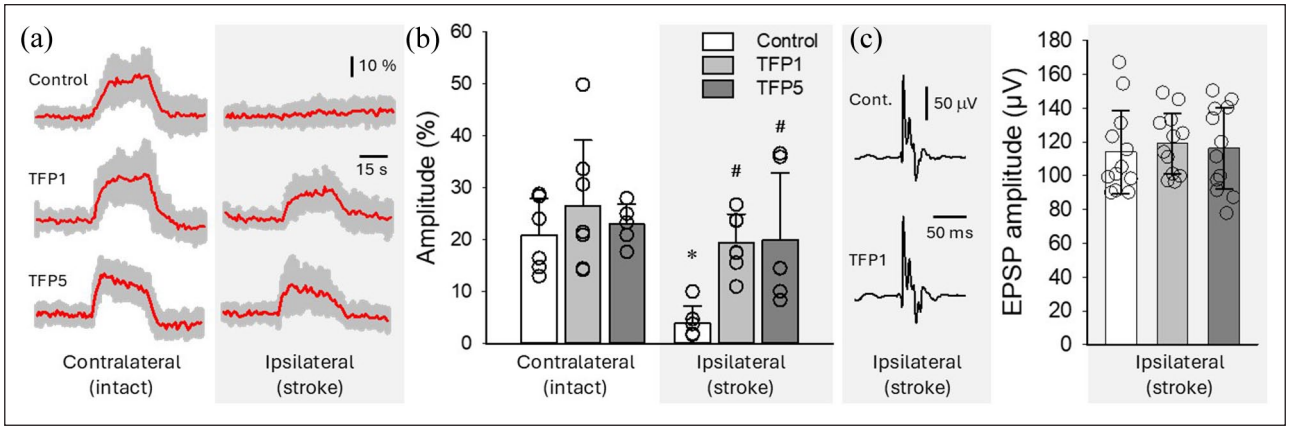

Figure 2. TFP rescues neurovascular coupling: (a) mean traces of functional hyperemia (with stdev in gray) in response to somatosensory whisker stimulation illustrate that the hyperemic response was abolished after ischemia but restored by TFP treatment, (b) the relative amplitude of functional hyperemia in response to whisker stimulation across hemispheres and experimental treatment regimens demonstrates the efficacy of TFP in rescuing the vascular response, and (c) the amplitude of EPSPs is shown in representative traces and was analyzed in the ischemic hemisphere of control and TFP1-treated mice, proving no TFP effect on neuronal activity. Data are presented as mean ± stdev, with individual data points overlaid. For each animal, the mean of three consecutive stimulations was used as a single value. After confirming normal distribution using the Shapiro–Wilk test, a two-way ANOVA (b; $^{**}F_{stroke} = 9.771$, $^{*}F_{treatment} = 5.285$) followed by a Sidak–Holms post hoc test or a one-way ANOVA (c; $F = 0.139$) was applied for statistical analysis. Significance was set at $^{*}p < 0.05$ (vs contralateral control) and $^{\#}p < 0.05$ (vs ipsilateral control).

EPSPs: excitatory postsynaptic potentials; TFP: trifluoperazine. The panel labels within the legend link the F values to the corresponding panels. For example: (b; etc. . . .) Significance labels for the post hoc test in panel b are given in the figure.

intact hemisphere; Figure 2(a) and (b)). The amplitude of excitatory postsynaptic potentials (EPSPs) in the ischemic hemisphere was similar between TFP1 and control groups (Figure 2(c)) and did not correspond to the magnitude of the hyperemic response, suggesting that TFP selectively enhanced cerebrovascular function.

TFP enhances the cerebral blood flow response to SD in the non-ischemic mouse cortex

Since the occurrence of SDs is common in AIS, reflects the excitability of brain tissue, and the magnitude of the CBF response to SD represents the state of vascular reactivity, we investigated whether TFP inhibits SDs or enhances the associated CBF response. These experiments were conducted in non-ischemic brains.

Both the frequency of KCl-induced SDs and their relative amplitude tended to be reduced by TFP (e.g. amplitude of the first SD in a train: 12.96 ± 7.05 vs 18.88 ± 2.64 mV, TFP vs control), although the reduction did not reach statistical significance (Figure 3(a)–(c)). TFP had no effect on the CBF response to the first SD in a train (peak: 118.9% ± 22.7% vs 112.7% ± 23.5%, TFP vs control). However, the amplitude of subsequent recurrent SDs exceeded baseline CBF levels in the TFP group (122.6% ± 23.5%), whereas it remained below baseline in controls (93.6% ± 26.7%; Figure 3(d) and (e)). This difference was remarkable for the area under the curve (AUC) of the hyperemic phase of the CBF response associated with recurrent SDs (9419.4% ± 2173.6% vs 5444.7% ± 1828.2% × s; TFP vs control; Figure 3(f)).

TFP attenuates SDs, preserves tissue integrity and downregulates AQP4 in brain slice preparations exposed to hypo-osmotic medium

Tissue swelling in brain slices was quantified as the increase in surface area relative to baseline measurements in aCSF. The hypo-osmotic medium (HM60), together with superimposed SD events, induced marked tissue swelling, which was reduced by approximately half following TFP treatment (Figure 4(a) and (b)). In the presence of TFP, spontaneous SDs were less likely to occur and exhibited a longer latency compared with HM60 alone (953 ± 463 vs 696 ± 336 s; HM60 + TFP vs HM60). SD latency, which was markedly shorter for anoxia-induced than for spontaneous SDs, was particularly prolonged in the presence of TFP compared with HM60 alone (71 ± 38 vs 42 ± 30 s; HM60 + TFP vs HM60; Figure 4(c)–(e)). Furthermore, the tissue area invaded by SDs, expressed as a percentage of total slice surface area, was significantly reduced in the TFP group for both spontaneous SDs (41.5% ± 12.4% vs 56.7% ± 13.8%; HM60 + TFP vs HM60) and anoxia-induced SDs (42.0% ± 11.3% vs 67.9% ± 12.8%; HM60 + TFP vs HM60; Figure 4(f)).

Tissue integrity, which was compromised under HM60 conditions, was preserved by TFP, as demonstrated by TTC staining and further supported by the increased

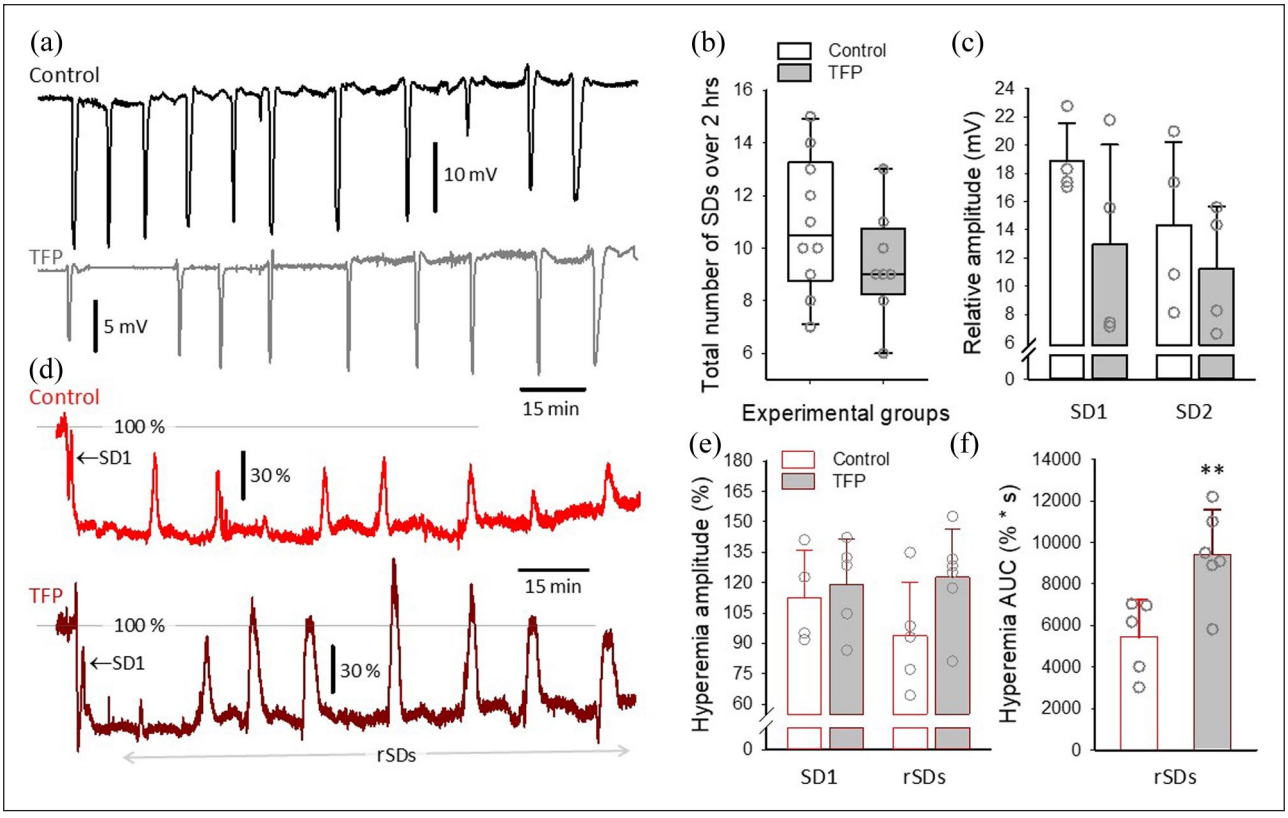

Figure 3. TFP augments hyperemia coupled with SD: (a) representative DC potential recordings from a control (upper trace) and a TFP-treated preparation (lower trace) illustrate the pattern of rSDs triggered by continuous exposure to topical KCl, (b, c) both the total number of SDs and the relative amplitude of the first (SD1) and second (SD2) events tended to be lower in the presence of TFP, although the differences did not reach statistical significance, (d) representative laser-Doppler flowmetry traces from a control (upper trace) and a TFP-treated preparation (lower trace) show the kinetics of the SD-coupled CBF response, and (e, f) the amplitude of hyperemia associated with rSDs showed a tendency to increase in the TFP group, with a significantly greater AUC. Data sets with discrete values (b) are presented as a box plot with individual data points overlaid and were analyzed using the Mann–Whitney test. The normality of data distribution was confirmed with the Shapiro–Wilk test (c, e, f), and normally distributed data are shown as mean ± stdev with individual data points overlaid. One-way ANOVA was applied for statistical analysis. Statistical significance was set at $^{**}p < 0.01$ (TFP vs control).
AUC: area under the curve; CBF: cerebral blood flow; DC: direct current; rSDs: recurrent SDs; SD: spreading depolarization; TFP: trifluoperazine.

relative area of NeuN-labeled neurons in TFP-treated slices (10.15% ± 2.31% vs 7.83% ± 2.36%, HM60 + TFP vs HM60; Figure 5(a) and (d)). Astrocytes stained for GFAP occupied a similar relative area in both the TFP-treated and control groups (4.37% ± 2.17% and 5.18% ± 4.85%, HM60 + TFP and HM60; Figure 5(b) and (d)). Importantly, AQP4 channel expression was decreased following TFP treatment, as indicated by the reduced relative tissue area immunopositive for AQP4 (1.88% ± 0.72% vs 3.66% ± 0.96%, HM60 + TFP vs HM60; Figure 5(c) and (d)).

Discussion

We set out to explore whether administration of TFP, a calmodulin inhibitor that was previously shown to block AQP4 translocation to the astrocytic plasma membrane,[16,22] could inhibit cytotoxic edema formation during the early phase of AIS, limit infarct maturation, and improve the recovery of neurological and cerebrovascular function. Our therapeutic approach in AIS mice was designed to offer translational relevance, as TFP was delivered as a post-treatment, with administration initiated after recanalization. Moreover, TFP administration was targeted to the hyperacute phase, when cytotoxic edema formation is prominent and the risk of interfering with later edema resolution is minimal. The post-recanalization application of TFP is reversible, as inhibition of AQP4 translocation is lifted once the drug is cleared, thereby allowing AQP4-mediated edema resolution at later time points. Finally, bolus administration upon recanalization (TFP5), as opposed to repeated daily administration (TFP1), proved more beneficial, as shown by the reduction in infarct volume (Figure 1(b)), while maintaining equal efficacy in neurovascular coupling (Figure 2) and functional outcomes (Figure 1(f)). This may highlight the dynamic

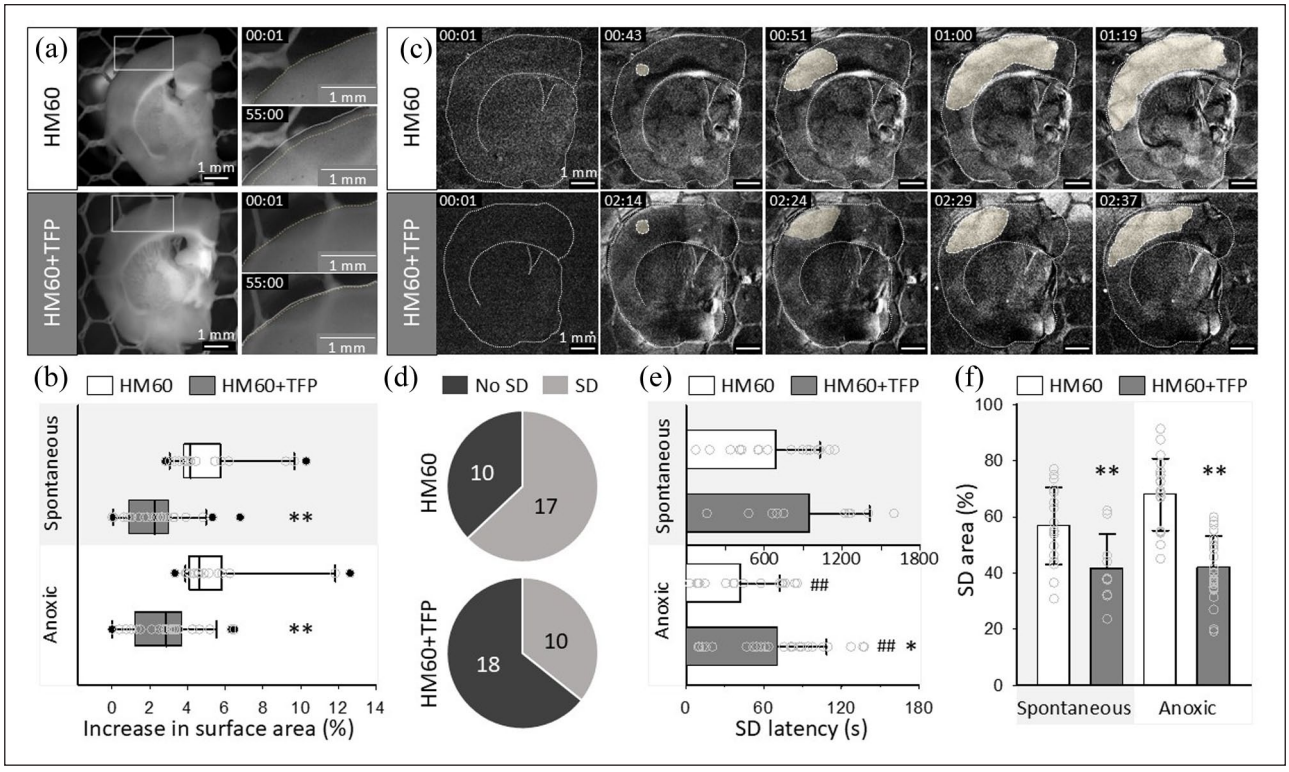

Figure 4. TFP mitigates brain slice swelling and SDs under hypo-osmotic challenge: (a) representative IOS images demonstrating brain slice swelling in HM60 alone or with the addition of TFP (HM60 + TFP). Tissue swelling is indicated by the displacement of the contour of the parietotemporal cortex in each condition (insets). The time stamp is shown as min:s, (b) increase in the surface area of brain slices relative to baseline, measured after spontaneous SDs (40 min after the start of HM60 or HM60 + TFP incubation) and SDs triggered by anoxia (55 min after the start of incubation). The time stamp is shown as min:s, (c) representative, background subtracted, IOS image sequences showing the latency of anoxic SD occurrence. Note the increased latency and reduced area covered by SDs in HM60 + TFP compared to HM60, (d) frequency of spontaneous SDs in HM60 versus HM60 + TFP. SDs occurred less frequently in the presence of TFP, (e) latency of spontaneous and anoxic SDs, relative to the onset of HM60 or HM60 + TFP incubation and anoxia induction, respectively, and (f) cortical surface area covered by SD relative to total area. Normality of data in panels (b, e, f) was evaluated using the Shapiro–Wilk test. For normally distributed data (e, f), data are presented as mean ± stdev, with individual data points overlaid, and two-way ANOVA (factors: SD type and treatment) was applied, followed by Sidak's post hoc test. Non-normally distributed data (b) are shown as box plot with individual data points overlaid, and were analyzed using the Mann–Whitney test. The cutoff for significance was set at $^{*}p < 0.05$ and $^{**}p < 0.01$ HM60 + TFP versus HM60, and $^{\#\#}p < 0.01$ anoxic versus spontaneous SD.
HM: hypoosmotic medium; IOS: intrinsic optical signal; SD: spreading depolarization; TFP: trifluoperazine.

nature of edema formation and the importance of targeting its very early phase, while minimizing interference with edema resolution.

In contrast to the expectations, neither bolus nor repeated TFP treatment following MCAO resulted in a reduction of edema size as assessed by MRI. Importantly, however, infarct volume was significantly reduced in line with recent evidence[35] and neurological outcomes improved, particularly when TFP was administered as a bolus immediately after recanalization (Figure 1). Yet, data obtained from our osmotically challenged acute brain slice preparations, used to gain mechanistic insight, demonstrated that tissue swelling and AQP4 immunolabeling were reduced in the presence of TFP (Figures 4 and 5). The apparent discrepancy in TFP's effects on edema formation in the two models is likely attributable to differences in the timing of the experimental endpoints. In acute brain slices, the observation period was limited to 60 min after the insult in the continued presence of TFP, whereas AIS mice underwent neuroimaging to evaluate edema and infarct size 3 days after MCAO and bolus TFP administration. We propose that the brain slice experiments predominantly captured the effect of TFP on acute osmotic stress and cytotoxic edema,[32] while MRI performed 3 days after MCAO reflected the additional, delayed contribution of vasogenic edema.[8,9] This interpretation is further supported by our findings showing that BBB leakage, assessed by SPECT, was not affected by TFP (Figure 1). This appears to be in contrast to a previous report demonstrating BBB protection by TFP in immortalized mouse brain microvascular endothelial cells under ischemic conditions.[35] Still, TFP was beneficial in both of our

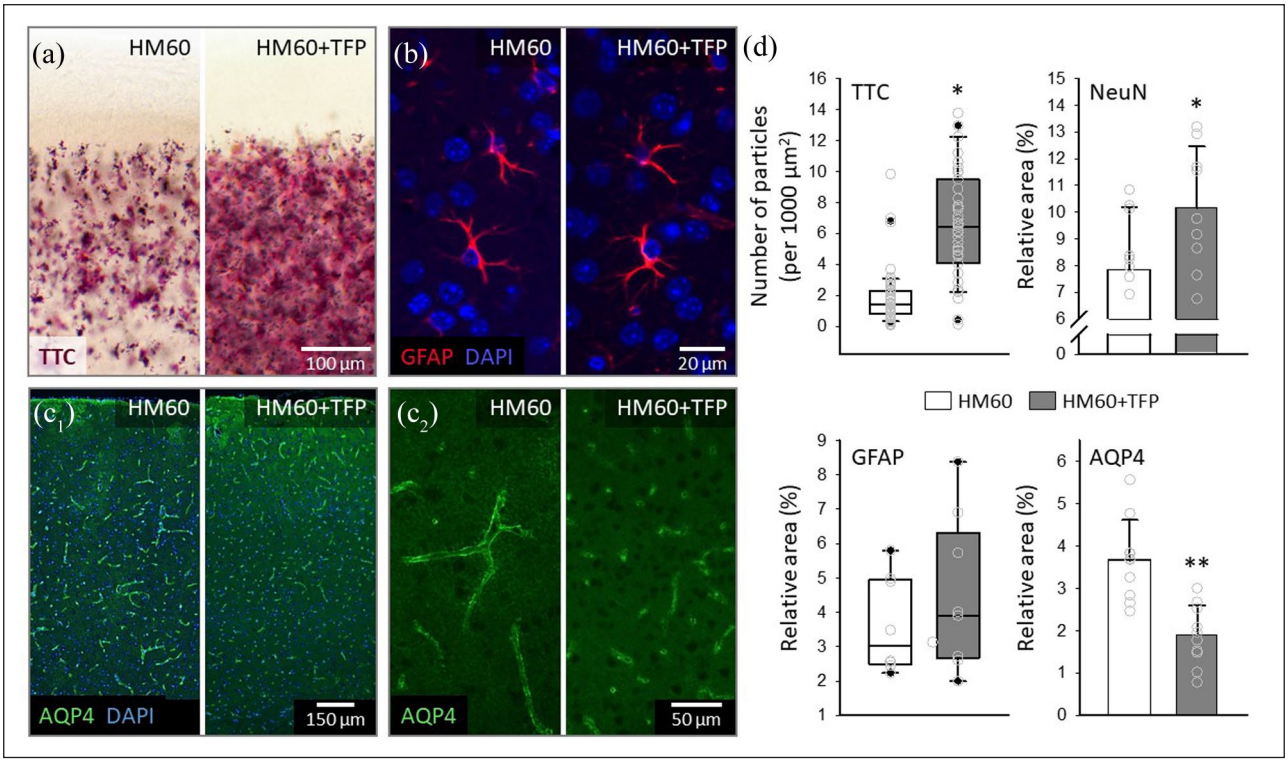

Figure 5. TFP prevents tissue injury and represses AQP4 expression in osmotically challenged brain slice preparations: (a) TTC-stained sections represent tissue viability, with fewer TTC-positive cellular compartments (i.e. particles) indicating decreased tissue viability, (b) reactive astrocytes immunolabeled for GFAP did not display treatment-related alterations, (c) fluorescent images immunostained for AQP4 showed reduced and more fragmented signal in TFP-treated slices, and (d) quantitative analysis of the histological findings evaluated the number of TTC-stained particles per standard surface area, as well as the immunopositive area (NeuN, GFAP, or AQP4) relative to the total cortical surface. Normality of data was evaluated using the Shapiro–Wilk test. Non-normally distributed data are shown as box plots with individual data points overlaid and were analyzed using the Mann–Whitney test. Normally distributed data are presented as mean ± stdev with individual data points overlaid and were analyzed with a one-way ANOVA. The cutoff for significance was set at $*p < 0.05$ and $**p < 0.01$ HM60 + TFP versus HM60.
AQP4: aquaporin-4; GFAP: glial fibrillary acidic protein; TFP: trifluoperazine; TTC: triphenyl tetrazolium chloride.

experimental models in protecting against neural injury, as evidenced by reduced infarct size after MCAO (Figure 1) and a greater number of NeuN-positive cells in brain slice preparations (Figure 5). In addition, TFP promoted functional recovery as shown with the GNS test (Figure 1). Taking these results together, we argue, in light of our additional cerebrovascular findings, that TFP exerts neuroprotective effects possibly by improving cerebrovascular function, either in addition to, or as a consequence of, counteracting astrocyte swelling.

Indeed, we found that TFP greatly improved neurovascular coupling in ischemic tissue after MCAO (Figure 2), as well as the CBF response to SD in the optimally perfused cortex (Figure 3). Astrocytes are intimately apposed to the microvascular wall, covering more than 95% of the vascular surface with their endfeet where AQP4 is abundantly expressed, and are essential regulators of vascular tone during neurovascular coupling with somatosensory stimulation.[36] Likewise, astrocytes play a pivotal role in shaping the CBF response to SD[37] and are heavily implicated in SD itself.[38] Adding further complexity, SD is accompanied by astrocytic swelling[39] and contributes to cytotoxic edema with the involvement of AQP4.[13,24] Swelling of astrocytic endfeet compresses the microvasculature, occurring within an hour after acute brain injury, peaking around 6 h post-impact, and gradually resolving by approximately day 3, as described in human samples.[40] This physical compression is understood to increase capillary transit time heterogeneity, which can critically reduce oxygen availability.[40] We suggest that targeting AQP4 and thus reducing astrocyte swelling with TFP may therefore contribute to the observed improvement in cerebrovascular function by relieving the physical compression of cerebral vessels. Further cytomorphological analyses should help clarify this possibility.

Alternatively, ischemia and cytotoxic edema may disrupt the neurochemical machinery underlying astrocytic vasoregulation. Astrocytes release both vasodilatory (prostaglandin E_2 (PGE_2)) and vasoconstrictive (20-hydroxyeicosatetraenoic acid (20-HETE)) metabolites of arachidonic acid in various contexts, with 20-HETE synthesis being markedly increased in association with increased

microvascular tone in ischemic brain tissue and during SD.[41–43] Although no experimental evidence currently indicates that astrocytic cytotoxic edema directly drives increased 20-HETE synthesis, both AQP4 translocation to the plasma membrane and 20-HETE production are mechanistically linked to astrocytic Ca^{2+} oscillations that are augmented by ischemia.[22,42,43] It is therefore conceivable that TFP, in addition to its inhibition of AQP4 translocation and the resulting attenuation of swelling, suppresses astrocytic vasoconstrictor signaling or rescues vasodilator signaling, thereby shifting the balance toward decreased microvascular tone.

In our acute brain slice preparations challenged by osmotic stress, we observed that SD occurred with decreased frequency, prolonged latency, and a shorter propagation distance in the presence of TFP (Figure 4). A similar tendency was noted in vivo, as well (Figure 3). This may represent a mechanistic correlate of the tissue integrity preserved by TFP, because SD in injured tissue is known to promote the expansion of irreversible damage,[23] and therefore SD inhibition is expected to prevent the exacerbation of neuronal cell loss.[34] Consistent with our present findings, we previously demonstrated that osmotic challenge, and the resulting tissue swelling, renders brain tissue increasingly susceptible to SD, an effect that can be reversed by the combined pharmacological antagonism of water influx driven by Na^+–K^+–$2Cl^-$ cotransporters and mediated by AQP4 (TGN-020 and bumetanide).[32] The blockade of excessive water influx into astrocytes is thought to preserve their spatial buffering capacity, which is critical for both delaying SD initiation and facilitating SD termination.[32,33,38] Together, the present and earlier data provide compelling evidence that mitigating cytotoxic edema by targeting astrocytic AQP4 inhibits SD, with putative neuroprotective consequences.

Limitations

A technical limitation of the experimental model is the restricted ability to assess the extent of spreading ischemia, the inverse and potentially detrimental CBF response associated with SD.[23,37] In the present experiments, MCAO was performed with the mouse in a supine position because vascular occlusion proved technically challenging when the animal was fixed in a stereotactic frame. The latter configuration would have allowed laser speckle contrast imaging to capture CBF responses associated with spontaneous SDs. As an alternative approach, we chemically induced spreading depolarizations in optimally perfused cortex. However, this approach involves the compromise that spreading ischemic responses are not expected to develop under such conditions.

Although our experimental work has yielded encouraging results demonstrating the efficacy of TFP in mitigating the consequences of AIS, its cellular mechanisms of action are complex, therefore potential side effects must be carefully weighed against its benefits. First, TFP is an FDA-approved antipsychotic agent and its therapeutic effect in schizophrenia comes mainly from dopamine D2-receptor blockade in specific brain pathways. It remains important to determine what concentration range provides ischemic neuroprotection through calmodulin modulation,[22] preferably without eliciting psychiatric effects. Second, given that TFP is known as a calmodulin inhibitor, and calmodulin participates in a wide array of intracellular signaling pathways,[44] the consequences of its transient systemic inhibition are complex and not yet fully understood. Among other effects, TFP-mediated calmodulin inhibition may alter calcium release from the sarcoplasmic reticulum of ventricular cardiomyocytes.[45] This mechanism may underlie some of TFP's known cardiovascular adverse effects, including QT interval prolongation, an increased risk of arrhythmias, and orthostatic hypotension in susceptible individuals.[46] Such adverse effects could be particularly problematic in patients with AIS, who often present with cardiovascular comorbidities. Consistent with these concerns, a recent clinical study examined stroke risk among new users of typical and atypical antipsychotics, including TFP, by extending Sentinel tabulation analyses from individuals aged 18–64 years without dementia to adults aged 65 years and older irrespective of dementia status (ClinicalTrials.gov identifier: NCT04002700).

Despite these limitations, efforts to repurpose TFP for non-psychiatric indications are already underway. For example, TFP has recently been proposed as an antimetastatic chemotherapeutic agent[47] and as a treatment for glioblastoma based on its calmodulin-modulating properties.[48,49] In this context, TFP may also represent a therapeutic candidate for AIS, provided that its safety profile is carefully evaluated in this patient population.

Resource availability

This study did not generate new unique reagents. All materials used in this study are commercially available. Further information and requests for resources should be directed to and will be fulfilled by the corresponding authors, Dr. Eszter Farkas (farkas.eszter@szte.hu) and Dr. Ákos Menyhárt (menyhart.akos@szte.hu). Data supporting the findings of this study are available from the Corresponding Authors upon reasonable request.

Author contributions

RT: formal analysis, investigation, visualization, writing—review and editing. AT: formal analysis, investigation, visualization. MS: formal analysis, investigation, visualization, writing—review and editing. NK: methodology, formal analysis, visualization. IH: methodology, formal analysis, visualization. AEF: formal analysis, investigation, visualization. RF: supervision, formal analysis, writing—review and editing. KS: methodology, resources,

supervision. FB: supervision, writing—review and editing. IAK: resources, supervision, writing—review and editing. DM: methodology, resources, supervision, writing—review and editing, funding acquisition. ÁM: conceptualization, formal analysis, investigation, supervision, writing—review and editing, funding acquisition. EF: formal analysis, visualization, supervision, writing—original draft, funding acquisition.

Funding

The authors disclosed receipt of the following financial support for the research, authorship, and/or publication of this article: The EU's Horizon 2020 research and innovation program grant number 739593; the National Research, Development and Innovation Office of Hungary (grant numbers K146725, FK142218, K135425, STARTING_24 150356, HUN-REN RGH151414, and TKP2021-EGA-09); the János Bolyai Research Fellowship (BO/00254/25) and the National Brain Research Program 3.0 of the Hungarian Academy of Sciences; the Research Fund of the Albert Szent-Györgyi Medical School, University of Szeged, Hungary; and the University of Szeged Open Access Fund (nr. 8679).

Declaration of conflicting interests

The authors declared no potential conflicts of interest with respect to the research, authorship, and/or publication of this article.

ORCID iDs

Réka Tóth https://orcid.org/0000-0001-9066-5804
Ákos Menyhárt https://orcid.org/0000-0002-1355-3208
Eszter Farkas https://orcid.org/0000-0002-8478-9664

References

1. Feigin VL, Brainin M, Norrving B, et al. World Stroke Organization: global stroke fact sheet 2025. *Int J Stroke* 2025; 20(2): 132–144.
2. Battey TW, Karki M, Singhal AB, et al. Brain edema predicts outcome after nonlacunar ischemic stroke. *Stroke* 2014; 45(12): 3643–3648.
3. Ng FC, Yassi N, Sharma G, et al. Cerebral edema in patients with large hemispheric infarct undergoing reperfusion treatment: a HERMES meta-analysis. *Stroke* 2021; 52(11): 3450–3458.
4. Bardutzky J and Schwab S. Antiedema therapy in ischemic stroke. *Stroke* 2007; 38(11): 3084–3094.
5. Cook AM, Morgan Jones G, Hawryluk GWJ, et al. Guidelines for the acute treatment of cerebral edema in neurocritical care patients. *Neurocrit Care* 2020; 32(3): 647–666.
6. Peters NA, Farrell LB and Smith JP. Hyperosmolar therapy for the treatment of cerebral edema. *US Pharm* 2018; 43(1): HS-8–HS-11.
7. Burks SR, Kersch CN, Witko JA, et al. Blood–brain barrier opening by intracarotid artery hyperosmolar mannitol induces sterile inflammatory and innate immune responses. *Proc Natl Acad Sci U S A* 2021; 118(18): Article e2021915118.
8. Thrane AS, Rangroo Thrane V and Nedergaard M. Drowning stars: reassessing the role of astrocytes in brain edema. *Trends Neurosci* 2014; 37(11): 620–628.
9. Liebeskind DS, Jüttler E, Shapovalov Y, et al. Cerebral edema associated with large hemispheric infarction. *Stroke* 2019; 50(9): 2619–2625.
10. Tang G and Yang GY. Aquaporin-4: a potential therapeutic target for cerebral edema. *Int J Mol Sci* 2016; 17(10): Article 1413.
11. Nagelhus EA, Mathiisen TM and Ottersen OP. Aquaporin-4 in the central nervous system: cellular and subcellular distribution and coexpression with KIR4.1. *Neuroscience* 2004; 129(4): 905–913.
12. Andrew RD, Labron MW, Boehnke SE, et al. Physiological evidence that pyramidal neurons lack functional water channels. *Cereb Cortex* 2007; 17(4): 787–802.
13. Mestre H, Du T, Sweeney AM, et al. Cerebrospinal fluid influx drives acute ischemic tissue swelling. *Science* 2020; 367(6483): Article eaax7171.
14. Manley GT, Fujimura M, Ma T, et al. Aquaporin-4 deletion in mice reduces brain edema after acute water intoxication and ischemic stroke. *Nat Med* 2000; 6(2): 159–163.
15. Murata Y, Sugimoto K, Yang C, et al. Activated microglia-derived macrophage-like cells exacerbate brain edema after ischemic stroke correlate with astrocytic expression of aquaporin-4 and interleukin-1 alpha release. *Neurochem Int* 2020; 140: Article 104848.
16. Salman MM, Kitchen P, Halsey A, et al. Emerging roles for dynamic aquaporin-4 subcellular relocalization in CNS water homeostasis. *Brain* 2022; 145(1): 64–75.
17. Stokum JA, Kwon MS, Woo SK, et al. SUR1–TRPM4 and AQP4 form a heteromultimeric complex that amplifies ion/water osmotic coupling and drives astrocyte swelling. *Glia* 2018; 66(1): 108–125.
18. García Ríos CA and Leon-Rojas JE. Aquaporin-4 in stroke and brain edema—friend or foe?. *Int J Mol Sci* 2025; 26(17): Article 8178.
19. Ren Z, Iliff JJ, Yang L, et al. "Hit & Run" model of closed-skull traumatic brain injury (TBI) reveals complex patterns of post-traumatic AQP4 dysregulation. *J Cereb Blood Flow Metab* 2013; 33(6): 834–845.
20. Kitchen P, Day RE, Taylor LH, et al. Identification and molecular mechanisms of the rapid tonicity-induced relocalization of the aquaporin 4 channel. *J Biol Chem* 2015; 290(27): 16873–16881.
21. Glober NK, Sprague S, Ahmad S, et al. Acetazolamide treatment prevents redistribution of astrocyte aquaporin 4 after murine traumatic brain injury. *Neurosci J* 2019; 2019: Article 2831501.
22. Kitchen P, Salman MM, Halsey AM, et al. Targeting aquaporin-4 subcellular localization to treat central nervous system edema. *Cell* 2020; 181(4): 784–799.e19.
23. Hartings JA, Shuttleworth CW, Kirov SA, et al. The continuum of spreading depolarizations in acute cortical lesion development: examining Leão's legacy. *J Cereb Blood Flow Metab* 2017; 37(5): 1571–1594.
24. Dreier JP, Lemale CL, Kola V, et al. Spreading depolarization is not an epiphenomenon but the principal mechanism of the cytotoxic edema in various gray matter structures of

the brain during stroke. *Neuropharmacology* 2018; 134(Pt B): 189–207.
25. Kilkenny C, Browne W, Cuthill IC, et al. Animal research: reporting in vivo experiments: the ARRIVE guidelines. *Br J Pharmacol* 2010; 160(7): 1577–1579.
26. Tóth R, Szabó N, Törteli A, et al. The paradoxical relationship of sensorimotor deficit and lesion volume in acute ischemic stroke. *J Neuropathol Exp Neurol* 2025; 84(9): 771–779.
27. Koizumi J. Experimental studies of ischemic brain edema. A new experimental model of cerebral embolism in rats in which recirculation can be introduced in the ischemic area. *Jpn J Stroke*, 1986; 8: 1–8.
28. Garcia JH, Wagner S, Liu KF, et al. Neurological deficit and extent of neuronal necrosis attributable to middle cerebral artery occlusion in rats. Statistical validation. *Stroke* 1995; 26(4): 627–634; discussion 635.
29. Krafft PR, McBride DW, Lekic T, et al. Correlation between subacute sensorimotor deficits and brain edema in two mouse models of intracerebral hemorrhage. *Behav Brain Res* 2014; 264: 151–160.
30. Menyhárt Á, Bálint AR, Kozák P, et al. Nimodipine accelerates the restoration of functional hyperemia during spreading oligemia. *J Neurochem* 2024; 168(5): 888–898.
31. Menyhárt Á, Zölei-Szénási D, Puskás T, et al. Spreading depolarization remarkably exacerbates ischemia-induced tissue acidosis in the young and aged rat brain. *Sci Rep* 2017; 7(1): 1154.
32. Menyhárt Á, Frank R, Farkas AE, et al. Malignant astrocyte swelling and impaired glutamate clearance drive the expansion of injurious spreading depolarization foci. *J Cereb Blood Flow Metab* 2022; 42(4): 584–599.
33. Frank R, Bari F, Menyhárt Á, et al. Comparative analysis of spreading depolarizations in brain slices exposed to osmotic or metabolic stress. *BMC Neurosci* 2021; 22(1): 33.
34. Frank R, Szarvas PA, Pesti I, et al. Nimodipine inhibits spreading depolarization, ischemic injury, and neuroinflammation in mouse live brain slice preparations. *Eur J Pharmacol* 2024; 977: Article 176718.
35. Zhang W, Chen S, Ma B, et al. Trifluoperazine regulates blood–brain barrier permeability via the MLCK/p-MLC pathway to promote ischemic stroke recovery. *iScience* 2024; 27(3): Article 109156.
36. Attwell D, Buchan AM, Charpak S, et al. Glial and neuronal control of brain blood flow. *Nature* 2010; 468(7321): 232–243.
37. Ayata C and Lauritzen M. Spreading depression, spreading depolarizations, and the cerebral vasculature. *Physiol Rev* 2015; 95(3): 953–993.
38. Seidel JL, Escartin C, Ayata C, et al. Multifaceted roles for astrocytes in spreading depolarization: a target for limiting spreading depolarization in acute brain injury?. *Glia* 2016; 64(1): 5–20.
39. Risher WC, Croom D and Kirov SA. Persistent astroglial swelling accompanies rapid reversible dendritic injury during stroke-induced spreading depolarizations. *Glia* 2012; 60(11): 1709–1720.
40. Østergaard L, Engedal TS, Aamand R, et al. Capillary transit time heterogeneity and flow-metabolism coupling after traumatic brain injury. *J Cereb Blood Flow Metab* 2014; 34(10): 1585–1598.
41. Fordsmann JC, Ko RW, Choi HB, et al. Increased 20-HETE synthesis explains reduced cerebral blood flow but not impaired neurovascular coupling after cortical spreading depression in rat cerebral cortex. *J Neurosci* 2013; 33(6): 2562–2570.
42. Li Z, McConnell HL, Stackhouse TL, et al. Increased 20-HETE signaling suppresses capillary neurovascular coupling after ischemic stroke in regions beyond the infarct. *Front Cell Neurosci* 2021; 15: Article 762843.
43. Mishra A, Gordon GR, MacVicar BA, et al. Astrocyte regulation of cerebral blood flow in health and disease. *Cold Spring Harb Perspect Biol* 2024; 16(4): Article a041354.
44. Berchtold MW and Villalobo A. The many faces of calmodulin in cell proliferation, programmed cell death, autophagy, and cancer. *Biochim Biophys Acta* 2014; 1843(2): 398–435.
45. Qin J, Zima AV, Porta M, et al. Trifluoperazine: a ryanodine receptor agonist. *Pflugers Arch* 2009; 458(4): 643–651.
46. Buckley NA and Sanders P. Cardiovascular adverse effects of antipsychotic drugs. *Drug Saf* 2000; 23(3): 215–228.
47. Pulkoski-Gross A, Li J, Zheng C, et al. Repurposing the antipsychotic trifluoperazine as an antimetastasis agent. *Mol Pharmacol* 2015; 87(3): 501–512.
48. Kang S, Hong J, Lee JM, et al. Trifluoperazine, a well-known antipsychotic, inhibits glioblastoma invasion by binding to calmodulin and disinhibiting calcium release channel IP3R. *Mol Cancer Ther* 2017; 16(1): 217–227.
49. De Silva MI, Gan HK and Bardy C. Repurposing trifluoperazine for glioblastoma treatment. *Trends Pharmacol Sci* 2025; 46(5): 392–406.